

**Subpixel rainfall  
analysis from a dense  
gauge network**

N. Peleg et al.

# Radar subpixel-scale rainfall variability and uncertainty: a lesson learned from observations of a dense rain-gauge network

**N. Peleg<sup>1</sup>, M. Ben-Asher<sup>2</sup>, and E. Morin<sup>3</sup>**

<sup>1</sup>Institute of Earth Sciences, Hebrew University of Jerusalem, Jerusalem, Israel

<sup>2</sup>Department of Geological & Environmental Sciences, Ben Gurion University of the Negev, Beer-Sheva, Israel

<sup>3</sup>Department of Geography, Hebrew University of Jerusalem, Jerusalem, Israel

Received: 11 December 2012 – Accepted: 19 December 2012 – Published: 2 January 2013

Correspondence to: N. Peleg (nadav.peleg@mail.huji.ac.il)

Published by Copernicus Publications on behalf of the European Geosciences Union.

Title Page

Abstract

Introduction

Conclusions

References

Tables

Figures

◀

▶

◀

▶

Back

Close

Full Screen / Esc

Printer-friendly Version

Interactive Discussion



## Abstract

Hydrological models for runoff estimations and flash-flood predictions are very sensitive to rainfall's spatial and temporal variability. The increasing use of radar and satellite data in hydrological applications, due to the sparse distribution of rain gauges over most catchments worldwide, requires improving our knowledge of the uncertainties of these data. In 2011, a new super-dense network of rain gauges, containing 27 gauges covering an area of about 4 km<sup>2</sup>, was installed near Kibbutz Galed in northern Israel. This network was established for a detailed exploration of the uncertainties and errors regarding rainfall variability in remote-sensing at subpixel-scale resolution. In this paper, we present the analysis of the first year's record collected from this network and from the Shacham weather radar. The gauge–rainfall spatial correlation and uncertainty were examined along with the estimated radar error. The zero-distance correlation between rain gauges was high (0.92 on the 1-min scale) and increased as the time scale increased. The variance of the differences between radar pixel rainfall and averaged point rainfall (the variance reduction factor – VRF) was 1.6 %, as measured for the 1-min scale. It was also found that at least four uniformly distributed rain stations are needed to represent the rainfall on the radar pixel scale. The radar–rain gauge error was mainly derived from radar estimation errors as the gauge sampling error contributed up to 22 % to the total error. The radar rainfall estimations improved with increasing time scale and the radar-to-true rainfall ratio decreased with increasing time scale. Rainfall measurements collected with this network of rain gauges in the coming years will be used for further examination of rainfall's spatial and temporal variability.

## 1 Introduction

Complex interactions exist between the spatial and temporal variability of rainfall and watershed hydrological responses (Morin et al., 2006). This has been demonstrated by several hydrological studies: Singh (1997) discussed how the spatial and temporal

HESSD

10, 1–32, 2013

### Subpixel rainfall analysis from a dense gauge network

N. Peleg et al.

Title Page

Abstract

Introduction

Conclusions

References

Tables

Figures

⏪

⏩

◀

▶

Back

Close

Full Screen / Esc

Printer-friendly Version

Interactive Discussion



5 variability of rainfall affects the runoff hydrograph and peak discharge; Arnaud et al. (2011) indicated that large catchments, on the scale of hundreds of square kilometers, are more sensitive than small catchments to uncertainties resulting from not considering the spatial variability of the rainfall; Zoccatelli et al. (2011) pointed out that the catchment response is sensitive to the rainfall's spatial variability, even for small catchment sizes (a few dozens of square kilometers), and that neglecting the spatial variability would affect runoff timing; Rozalis et al. (2010) established a hydrological model for flash-flood prediction and found it to be very sensitive to the temporal variability of the rainfall, affecting both runoff amount and peak discharge; Faures et al. (1995) indicated that knowing the spatial variability of convective rainfall is essential, even for catchments of very small scale (less than a few square kilometers) when conducting hydrological modeling.

10 Rainfall is usually measured for hydrological applications by rain-gauge networks, weather radars or satellites. Although rain gauges are the most commonly used source, they are often too sparsely distributed; only a few dense rain-gauge networks world-  
15 wide adequately cover entire catchments. Weather radar records rainfall at high spatial and temporal resolution (e.g.  $1.5 \text{ km}^2$  and 3 min – see Sect. 2), which is suitable for most hydrological modeling purposes. Satellite-based rainfall estimates can also be used for hydrological applications but they typically represent larger space and time  
20 scales and can potentially be applied to large catchments (as discussed by Nikolopoulos et al., 2010). The increasing use of radar and satellite data in hydrological applications requires improving our knowledge of the uncertainties of these data (see a recent discussion by Berne and Krajewski (2013) of current limitations and challenges in the use of weather radars in hydrology). A main difficulty in this regard is that remotely  
25 sensed rainfall estimates are provided in spatially averaged pixels (typically  $1\text{--}4 \text{ km}^2$ ) and no equivalent ground truth data are available because of the above-mentioned sparseness of rain-gauge networks (see extensive discussion by Krajewski and Smith, 2002). In 2003, Krajewski et al. (2003) declared that “new designs of the rain gauge networks should be considered” to learn more about the high-resolution variability of

---

**Subpixel rainfall analysis from a dense gauge network**N. Peleg et al.

---

[Title Page](#)[Abstract](#)[Introduction](#)[Conclusions](#)[References](#)[Tables](#)[Figures](#)[⏪](#)[⏩](#)[◀](#)[▶](#)[Back](#)[Close](#)[Full Screen / Esc](#)[Printer-friendly Version](#)[Interactive Discussion](#)

rainfall. Almost a decade later, Krajewski et al. (2010) summarized their paper by stating that “one key factor in solving the persistent problem of radar-rainfall uncertainties is the availability of dense rain gauge networks that could provide valuable information for modeling these uncertainties”. In 2011, a new super-dense network of rain gauges was installed in northern Israel. This network was established to explore in detail the uncertainties and errors caused by rainfall variability at remote-sensing subpixel resolution. This is the first step in continuing research to expand our knowledge of the spatial and temporal variability of rainfall at scales below 2 km.

Several studies have dealt with rainfall variability at pixel and subpixel scales: in 1998, Krajewski et al. (1998) recognized the need to establish rain-gauge networks at the radar subpixel scale to estimate radar-rainfall uncertainty. They deployed a network, which included 10 stations (see configuration in Krajewski et al., 2003), in the Iowa City Municipal Airport. Habib et al. (2001b) used this network to estimate the errors resulting from the use of tipping-bucket rain gauges with the aim of capturing the rainfall’s small-scale temporal variability. By fitting a nonparametric regression on rainfall data collected from 15 collocated rain gauges (EVAC PicoNet network, Oklahoma), Ciach (2003) analyzed the local random errors of tipping-bucket rain gauges on a smaller scale. Later, Ciach and Krajewski (2006) used the PicoNet to analyze the spatial correlation of the rainfall over a 3 km × 3 km area; Ciach and Krajewski (1999) introduced the error separation method which allows distinguishing the rain-gauge sampling error from the radar rainfall estimation error. They used a network of five rain gauges with a scale similar to that of the radar pixel. Data from the PicoNet were used also by Seo and Krajewski (2011) to test the assumption that the covariance between radar rainfall error and rain gauge error in representing the radar sampling domain is negligible when using the error separation method. Two dense networks of eight gauges within a 4-km<sup>2</sup> grid located at the Brue catchment were used by Wood et al. (2000) to estimate the errors of the individual gauge and radar compared to the “true” mean areal rainfall. This network was later used by Villarini et al. (2008) to assess the errors resulting from temporal gaps in rainfall observations and the uncertainties resulting from

# HESSD

10, 1–32, 2013

## Subpixel rainfall analysis from a dense gauge network

N. Peleg et al.

Title Page

Abstract

Introduction

Conclusions

References

Tables

Figures



Back

Close

Full Screen / Esc

Printer-friendly Version

Interactive Discussion



areal-to-point estimations. Habib et al. (2001a) estimated the correlation coefficient of point rainfall using a clustered network of rain gauges deployed in Florida (TEFLUN-B network). Gebremichael and Krajewski (2004) used both TEFLUN-B and TRMM-LBA networks to estimate the radar's ability to characterize the small-scale spatial variability of rainfall by comparing the correlation function of the gauge and the radar. A network consisting of nine optical rain gauges within 500 m × 500 m was deployed in Denmark by Jensen and Pedersen (2005) to explore the radar subpixel-scale rainfall variation. Pedersen et al. (2010) used the same network to determine the coefficient of variation and the spatial correlation of the rainfall field. Fiener et al. (2009) installed a network consisting of 13 tipping-bucket rain gauges on a 1.4-km<sup>2</sup> area in Germany to determine the spatial variability of rainfall on a subkilometer scale, taking into account the wind's potential effect. The Walnut Gulch Experimental Watershed (WGEW), equipped with about 10 rain gauges per every TRMM Precipitation Radar pixel (~ 5 km in diameter), was used by Amitai et al. (2012) who conducted rain rate comparisons of these two resources for a semiarid climate. Several studies have explored the small-scale spatial variability of the rainfall drop size distribution (DSD) (Tapiador et al., 2010; Tokay et al., 2010). Jaffrain et al. (2011) deployed 16 optical disdrometers over a 1 km × 1 km area in Switzerland and determined the coefficient of variation of the total concentration of drops, the mass-weighted diameter and the rain rate over the network.

In the current study we set up the first step toward estimating the spatial subpixel sampling uncertainties and the errors of weather radar rainfall estimates using a super-dense rain-gauge network. The paper is composed of five sections: Section 2 is dedicated to technical information regarding the rain gauge network's installation and data quality control (QC). This section also contains information about the weather radar and rainfall estimations. The rainfall spatial correlation is described in Sect. 3. The uncertainty quantification for the mean areal rainfall representing the subpixel level is discussed in Sect. 4. The radar rainfall error variance and the radar evaluation are presented in Sect. 5. The conclusions of the paper and the near-future plans for the rain-gauge network are presented in Sect. 6.

---

## Subpixel rainfall analysis from a dense gauge network

N. Peleg et al.

---

[Title Page](#)[Abstract](#)[Introduction](#)[Conclusions](#)[References](#)[Tables](#)[Figures](#)[⏪](#)[⏩](#)[◀](#)[▶](#)[Back](#)[Close](#)[Full Screen / Esc](#)[Printer-friendly Version](#)[Interactive Discussion](#)

## 2 Data

### 2.1 Galed dense rain-gauge network

A very dense network of rain gauges was deployed in November 2011 near Kibbutz Galed, about 15 km east of northern Israel's coastline (Fig. 1). The network consists of 27 rain gauges, maintained by the Hydrometeorology Lab of the Hebrew University of Jerusalem, and one additional rain gauge operated by the Israel Meteorology Service. The rain gauges are deployed in 14 stations (coupled gauges per station, as in the Iowa network, Krajewski et al., 2003) covering an area of about 4 km<sup>2</sup> in the fields surrounding the Kibbutz (Fig. 1). This network differs spatially, but is in a similar range as the networks used in previous studies, for example: the EVAC PicoNet in Oklahoma City with 25 rain stations deployed over 9 km<sup>2</sup> (Ciach and Krajewski, 2006), the Scheyern Experimental Farm with 10 rain gauges over 1.4 km<sup>2</sup> (Fiener et al., 2009), the Aarhus network consisting of 9 gauges equally spaced within a 0.25-km<sup>2</sup> area (Jensen and Pedersen, 2005; Pedersen et al., 2010) or the 8 gauges deployed in a 4-km<sup>2</sup> area of the Brue catchment (Villarini et al., 2008).

The stations are distributed in a nonuniform design (Fig. 1), according to the terrain's limitations (e.g. field crops, small streams, woods). The intra-distances of the rain stations (see Table 1) vary between 57 m and 2,672 m. Each station consists of two high-precision tipping-bucket rain gauges separated by about 1 m (as suggested by Ciach and Krajewski, 1999; Krajewski et al., 2003) to maintain better quality control and to acquire data on the zero-distance correlation of the rainfall. The tipping-bucket rain gauge was manufactured by YOUNG Company (model 52203). It has an orifice diameter of 18 cm with rainfall measurement resolution of 0.1 mm per tip and accuracy of 3% up to 50 mm h<sup>-1</sup>. Each rain gauge is connected to a HOBO data logger (model UA-003-64). The maximum input frequency of the data logger is 1 pulse s<sup>-1</sup>, with a memory of 64 K bytes (more than enough for 1 yr of measurements). This stands with the recommendations by Habib et al. (2001b) and Wang et al. (2008) to use a gauge bucket size of up to 0.254 mm with a temporal resolution of 1 s.

HESSD

10, 1–32, 2013

### Subpixel rainfall analysis from a dense gauge network

N. Peleg et al.

Title Page

Abstract

Introduction

Conclusions

References

Tables

Figures

◀

▶

◀

▶

Back

Close

Full Screen / Esc

Printer-friendly Version

Interactive Discussion



---

**Subpixel rainfall  
analysis from a dense  
gauge network**N. Peleg et al.

---

[Title Page](#)[Abstract](#)[Introduction](#)[Conclusions](#)[References](#)[Tables](#)[Figures](#)[⏪](#)[⏩](#)[◀](#)[▶](#)[Back](#)[Close](#)[Full Screen / Esc](#)[Printer-friendly Version](#)[Interactive Discussion](#)

The study area has a Mediterranean climate; its rainy season lasts from October to May (mean annual rainfall is 550 mm), while June to September are typically dry and hot. In this study, we present the analysis of the first year record collected from 01 November 2011 to 01 May 2012. The accumulated rainfall for this period is equal to 512 mm (averaged over the rain gauges) and is divided into 63 rain events. A rain event is defined as beginning when the first rain tip is detected in one of the rain gauges and ending when there is an intermission of more than 15 min in rainfall for all gauges. Rain events with cumulative rainfall depth of less than 0.5 mm for all gauges were excluded. An inherent problem with tipping-bucket-derived rain intensities is that only the time at which the bucket is completely filled is recorded and no information is available on the actual period of time it took to get filled. To overcome this problem, a backward linear interpolation to the previous recorded tip was applied, with two exceptions: (1) the time interval from the previous tip was larger than 15 min, or (2) this was the first tip in the rain event. Note that low rain intensities are more vulnerable to the above-mentioned problem.

To ensure reliability of the results, QC procedures were conducted. This is essential as the data collected from the rain gauges may be corrupted due to partial clogging of the funnel by debris or small living creatures (for example, wasps or snails), or technical problems (such as a low battery) resulting in lack of measurements at a given time. Most of the errors were detected by comparing the rain intensity of rain gauge couples at each station and the rain event. In addition, the rain intensities of all of the gauges were compared for each rain event. All data which were considered to be corrupted were removed during the QC, ensuring a lack of intra- and inter-station measurement errors. After QC, rain intensity time series for time intervals between 1 min and daily time scales were computed for each rain gauge.

## 2.2 Radar data

Data from the Shacham (EMS) Mekorot company weather radar system located at Ben Gurion Airport, about 63 km south of the study area, were used in this study.

Data from this radar have been used extensively for climatology and hydrology studies over the last decade (see Karklinsky and Morin, 2006; Morin et al., 2001; Morin and Gabella, 2007; Morin et al., 2009; Peleg and Morin, 2012; Rozalis et al., 2010; Yakir and Morin, 2011). The radar is a C-band (5.35-cm wavelength), non-Doppler system with a maximal transmitting power of 250 kW, a temporal resolution of about 3 min per volume scan, and a spatial polar resolution of  $1.4^\circ \times 1$  km in space (see grid in Fig. 1). Data from an elevation angle of  $0.5^\circ$  (mean elevation of 710 m above ground) were used for the analysis. No pixels with substantial ground clutter or beam blockage were detected in the analyzed region.

A total of 11 827 radar volume scans were analyzed in this study. The radar was shut down by the EMS for short periods due to malfunctions and for regular maintenance, and thus 462 mm of rainfall were recorded by the radar out of the full 512 mm rainfall recorded by the rain gauges for the same period. We chose 12 radar pixels over the network location and its surroundings for the analysis (Fig. 1) as the area of the gauge network is similar to that of 2–4 joint radar pixels (approximately  $4 \text{ km}^2$ ).

Rainfall intensity data ( $R$ ,  $\text{mm h}^{-1}$ ) were calculated from the weather radar reflectivity data ( $Z$ ,  $\text{mm}^6 \text{ m}^{-3}$ ) by a fixed  $Z$ – $R$  power law relationship adjusted for each of the 12 radar pixels using the annual cumulative rainfall amount derived from the dense rain-gauge network. The  $Z$ – $R$  relationships were varied from  $Z = 55R^{1.5}$  to  $Z = 133R^{1.5}$  for the radar pixels, as summarized in Table 2. Prior to this adjustment, the radar reflectivity values were increased by 6 dB to compensate for system losses, as done by Morin and Gabella (2007). A lower threshold of  $0.1 \text{ mm h}^{-1}$  for noise filtering and an upper threshold of  $250 \text{ mm h}^{-1}$  to reduce unrealistically strong returns from hail particles were set.

In Fig. 2, scatter plots of synchronous radar (averaged data from the 12 pixels) and rain gauge observations are presented for three time scales: 3-min (the time interval between the radar volume scans), hourly and daily intervals. Ciach and Krajewski (1999) noted that this plot can give an idea of the large amount of variability in the measurements. Here we can see that for the shorter temporal resolution and for the lower

---

## Subpixel rainfall analysis from a dense gauge network

N. Peleg et al.

---

[Title Page](#)[Abstract](#)[Introduction](#)[Conclusions](#)[References](#)[Tables](#)[Figures](#)[◀](#)[▶](#)[◀](#)[▶](#)[Back](#)[Close](#)[Full Screen / Esc](#)[Printer-friendly Version](#)[Interactive Discussion](#)

rain intensity, the points scatter away from the perfect match line of the radar-to-gauge amounts, possibly due to the problem mentioned in the previous section.

### 3 Spatial correlation of gauge rainfall data

The spatial rainfall correlation is commonly investigated using Pearson's product-moment correlation (for examples, see Ciach and Krajewski, 2006; Mandapaka et al., 2010; Pedersen et al., 2010; Tokay and Ozturk, 2012; Villarini et al., 2008, and more). Correlograms for different time scales, from 1 min to daily, were computed using a lag distance of 200 m (Fig. 3). As expected, the spatial correlation decreased as the separation distance increased and as the time scale decreased. This trend was also shown by Krajewski et al. (2003) for several different experiments conducted worldwide, as well as by Ciach and Krajewski (2006) and Villarini et al. (2008). The correlation was parameterized using a three-parameter exponential function (see fit in Fig. 3), as suggested by Gebremichael and Krajewski (2004), Habib et al. (2001a) and Villarini et al. (2008), for the spatial correlation at separation distance  $h$  of the correlogram:

$$r(h) = c_1 \cdot \exp \left[ - \left( \frac{h}{c_2} \right)^{c_3} \right] \quad (1)$$

where  $c_1$  represents the zero-distance correlation (nugget),  $c_2$  is the correlation distance and  $c_3$  is the shape factor.

The time dependence of the parameters given in Eq. (1) are summarized in Fig. 4. The nugget has a value of about 0.92 on the 1-min scale, increasing to 0.98 for the 5-min scale and then continuing asymptotically toward the daily scale. The nugget represents the zero-distance correlation, thus it gives us information about the variability and measurement errors for each coupled rain gauge (i.e. each station); when  $c_1$  is equal to 1 there is a perfect match between the coupled gauges. The values obtained in this study were much higher than those reported by Villarini et al. (2008) of  $c_1 = 0.5$  on the 1-min time scale; they are on a scale similar to the values given by Krajewski

## Subpixel rainfall analysis from a dense gauge network

N. Peleg et al.

Title Page

Abstract

Introduction

Conclusions

References

Tables

Figures

◀

▶

◀

▶

Back

Close

Full Screen / Esc

Printer-friendly Version

Interactive Discussion



et al. (2003) of  $c_1 = 0.95\text{--}0.97$  (different locations worldwide) on time scales of 15 min or longer. The networks used in these studies were without coupled gauges, making it difficult to estimate the nugget parameter. Where coupled gauges have been used, the estimated nugget value is in closer agreement to the values obtained in this study, for example: Tokay and Ozturk (2012) reported values of  $c_1 = 0.97$  on a 5-min time scale.

The correlation distance ( $c_2$ ) increased with the time scale from 3 km to 79 km. The correlation distance for 12 h (79 km) was much lower than the value of 110 km estimated by Villarini et al. (2008) or the value of 320 km estimated by Tokay and Ozturk (2012). As the spatial scale in this study is limited to a distance of a few kilometers because of the network dimensions, we should interpret these very large correlation distances with caution, as was also mentioned by Tokay and Ozturk (2012).

In this study, the shape parameter ( $c_3$ ) was approximately 1 (a pure exponential function), slightly changing from 0.9 to 1.2 with no obvious trend. The shape parameter function estimated in this study was different from those obtained by Ciach and Krajewski (2006), Tokay and Ozturk (2012), and Villarini et al. (2008), where an increase in the shape parameter was detected with an increase in the time scale (between 1.1 and 1.6, 0.37 and 0.92 and 0.4 and 1, respectively). As Villarini et al. (2008) mentioned, differences are expected between experimental studies due to differences in the range of inter-gauge distances, sample size and precipitation type.

## 4 Spatial rain gauge uncertainty

### 4.1 Variance reduction factor

The rainfall variance was estimated by the well-known variance reduction factor (VRF), which has been used by Krajewski et al. (2000) and Villarini et al. (2008) to quantify the uncertainty results from averaging a number of rain gauges. The VRF methodology was introduced by Morrissey et al. (1995) who considered the number of rain gauges, their spatial distribution, and the correlation between them. In this paper, we provide

## Subpixel rainfall analysis from a dense gauge network

N. Peleg et al.

Title Page

Abstract

Introduction

Conclusions

References

Tables

Figures

◀

▶

◀

▶

Back

Close

Full Screen / Esc

Printer-friendly Version

Interactive Discussion



only a brief discussion of the VRF methodology; for further details, the reader is referred to the above-mentioned papers.

Let  $R_s$  be the point rainfall of a single rain station (coupled gauges per station), and let  $\overline{R_s}$  be the mean areal rainfall. The variance of the mean areal rainfall can be expressed as:

$$\sigma_{\overline{R_s}}^2 = \sigma_{R_s}^2 \cdot \text{VRF} \quad (2)$$

where  $\sigma_{R_s}^2$  is the variance of the point rainfall and the VRF is computed by:

$$\begin{aligned} \text{VRF} = & \frac{1}{n^2} \cdot \sum_{i=1}^N \sum_{j=1}^N \rho(d_{i,j}) \cdot \delta(i) \cdot \delta(j) \\ & - \frac{2}{N \cdot n} \cdot \sum_{i=1}^N \sum_{j=1}^N \rho(d_{i,j}) \cdot \delta(i) + \frac{1}{N} + \frac{2}{N^2} \cdot \sum_{i=1}^{N-1} \sum_{j=i+1}^N \rho(d_{i,j}) \end{aligned} \quad (3)$$

where  $n$  is the number of rainfall measuring stations,  $N$  is the number of boxes dividing the domain,  $\rho(d_{i,j})$  is the correlation coefficient derived from Eq. (1) for the distance between boxes  $i$  and  $j$ , and is a Boolean value with a value of 1 when box  $i$  contains a measuring station (each box can contain only one measuring station) and a value of 0 otherwise.

The domain area was defined with dimensions of 2.1 km  $\times$  2.1 km in order to capture all of the rain stations ( $n = 14$ ) participating in this study (Fig. 1; see the 4-km<sup>2</sup> box for comparison). The grid was composed of 441 boxes ( $N$ ), each with a size of 100 m  $\times$  100 m. The results are plotted in Fig. 5a. The VRF was 1.6 % for a time scale of 1 min and it decreased with increasing time accumulated to 0.07 % for the daily time scale. These results are similar to those presented by Villarini et al. (2008) for a 4-km<sup>2</sup> domain, where the VRF decreased from approximately 2.7 % for a time scale of 1 min to near zero for the daily time scale. The VRF is very close to zero, meaning that the

## Subpixel rainfall analysis from a dense gauge network

N. Peleg et al.

Title Page

Abstract

Introduction

Conclusions

References

Tables

Figures

◀

▶

◀

▶

Back

Close

Full Screen / Esc

Printer-friendly Version

Interactive Discussion





more moderately to 0.7 at the same distance. The nonconvective spatial correlation decays in a manner similar to the 5-min correlation decay of the combined convective and nonconvective rainfall presented in Fig. 3. The fast decay of the convective rainfall spatial correlation implies that the areal rainfall variance is high. The standard deviation of the convective rainfall, normalized by its mean, was plotted against the percentage of rain gauges exceeding the threshold of  $10 \text{ mm h}^{-1}$  (Fig. 6b). The normalized standard deviation (NSTD) of the convective rainfall is about 0.4. The maximum NSTD is higher for fewer rain gauges that detect rain intensity exceeding the threshold.

## 5 Radar estimation error

### 5.1 Error separation method

Ciach and Krajewski (1999) proposed the error separation method (ESM) which separates the radar-rain gauge error in two: the radar-true area-averaged rainfall error and the rain gauge sampling error. Below is a short description of the method; for further information the reader is referred to Ciach and Krajewski (1999) and to an additional example by Krajewski et al. (2000).

Let  $R_r$  be the rainfall estimated from the radar,  $R_g$  the rainfall as measured by the rain gauge and  $R_t$  the true area-averaged rainfall. The normalized root mean square error of the radar-estimated rainfall versus the rain gauges is found by:

$$\text{NRMSE}(R_r - R_g) = \frac{\sqrt{\frac{\sum_{i=1}^N (R_r(i) - R_g(i))^2}{N}}}{\bar{R}_g} \quad (4)$$

where  $N$  is the sample size and  $\bar{R}_g$  is the averaged rainfall measured by the gauges. The normalized rain gauge sampling error can be determined (based on Eq. (18) in

## Subpixel rainfall analysis from a dense gauge network

N. Peleg et al.

Title Page

Abstract

Introduction

Conclusions

References

Tables

Figures

◀

▶

◀

▶

Back

Close

Full Screen / Esc

Printer-friendly Version

Interactive Discussion



Ciach and Krajewski, 1999) by:

$$\text{NRMSE}(R_g - R_t) = \frac{\sqrt{\text{var}(R_g) \cdot (1 - c_1)}}{\bar{R}_g} \quad (5)$$

where  $c_1$  is the nugget. The radar–true area-averaged rainfall error can be then solved by:

$$\text{var}\{R_r - R_t\} = \text{var}\{R_r - R_g\} - \text{var}\{R_g - R_t\} \quad (6)$$

where  $\text{var}\{R_r - R_g\}$  and  $\text{var}\{R_g - R_t\}$  are derived from Eqs. (4) and (5), respectively. For the above computation, we assume that there is no bias between the rainfall measured by the rain gauges and the rainfall measured by the weather radar as each radar pixel is adjusted separately for the data derived from the gauges.

The results of the ESM for the different time scales are presented in Fig. 7 for the relative magnitude of each of the method components. The normalized radar–true rainfall error is presented for the maximum and minimum values obtained from the 12 radar pixels tested (i.e. maximum and minimum values represent one pixel each and the other 10 pixel values are found in the range between). The radar rain-gauge error declines from a maximum 700% error (minimum of 320%) for a time scale of 3 min to a maximum 65% error (minimum 47%) for the daily time scale. The error derived from the rain gauge sampling error is reduce from 71% for a time scale of 3 min to 5% for a daily time scale. The gauge sampling error contributes only a small part of the overall error: it changes from 22% (minimum contribution of 10%) for the 3-min time scale to 12% (minimum of 8.5%) for the daily time scale.

## 5.2 Radar rainfall evaluation

The radar rainfall was evaluated using the critical success index (CSI), false alarm ratio (FAR) and probability of detection (POD) parameters, all well-known parameters which

## Subpixel rainfall analysis from a dense gauge network

N. Peleg et al.

Title Page

Abstract

Introduction

Conclusions

References

Tables

Figures

◀

▶

◀

▶

Back

Close

Full Screen / Esc

Printer-friendly Version

Interactive Discussion



have been used in numerous studies (for example: Dixon and Wiener, 1993; Germann et al., 2006; Kyznarova and Novak, 2009). These quality parameters are defined as:

$$\text{CSI} = \frac{H}{H + F + M} \quad (7)$$

$$\text{FAR} = \frac{F}{H + F} \quad (8)$$

$$\text{POD} = \frac{H}{H + M} \quad (9)$$

where  $H$  is the number of hits – both radar and gauged areal average rainfall indicate rain,  $M$  means number of misses – rainfall was only recorded by rain gauges,  $F$  means false alarms – rainfall was only recorded by radar. A zero threshold was used to mark the occurrence of rain.

The evaluation was conducted for different time scales for each of the radar pixels and for the radar pixel average, and the results are presented in Fig 8. All quality parameters improved as the time scale increased, in a manner similar to the ESM results discussed in the previous section. The CSI for the averaged radar pixel changed from 0.56 for the 3-min time scale to 0.96 for the daily time scale and its POD increased from 0.73 to 0.96 for the same time scales. The FAR decreased from 0.29 for the 3-min time scale to zero for the 3-h time scale and on. These results are affected by the radar's lower threshold setting, where higher threshold changes the CSI, POD and FAR results. For some, but not all of the radar pixels, an improvement was detected.

The ratio of averaged radar rainfall to true areal rainfall was calculated for 3 min, 30 min and daily time scales. Here, we assumed that the true rainfall is well represented by the areal-averaged gauge-derived rainfall. The cumulative distribution (weighted by contribution to total rain amount) of the radar-to-true rainfall ratio (in dB) is presented in Fig. 9, following Germann et al. (2006). For the 3-min time scale, the radar underestimated about 76% of the rainfall, with the radar-to-true rainfall ratio reaching up to -20 dB. For the daily time scale, the radar estimations improved, with the inflection point between the under- and overestimation found around the 50% rainfall contribution

## Subpixel rainfall analysis from a dense gauge network

N. Peleg et al.

Title Page	
Abstract	Introduction
Conclusions	References
Tables	Figures
◀	▶
◀	▶
Back	Close
Full Screen / Esc	
Printer-friendly Version	
Interactive Discussion	



and the radar-to-true rainfall ratio being as low as  $-8$  dB. The improvement of the radar estimation for the true rainfall with increasing time scale was also expressed by the scatter parameter, defined as half the distance between the 16th and 84th percentiles of the error distribution (Germann et al., 2006). The scatter decreased from 4.67 dB for the 3-min time scale to 1.56 dB for the daily time scale.

## 6 Summary

Subpixel rain distribution was investigated using a high-density network of rain gauges as part of a continuous effort to better understand the uncertainties and errors of the rainfall estimation on this scale. This is of particular importance when using remote-sensing rainfall data (from ground weather radar or satellite) for hydrological applications. In this study, we used the network of 27 tipping-bucket rain gauges located in northern Israel to evaluate the Shacham weather radar's performance. The study conclusions can be summarized as follows:

- The zero-distance (nugget) correlation between rain gauges is high (0.92 on the 1-min scale) and it increases with increasing time scale. The overall rainfall correlations also increase with the time scale.
- The VRF decreases as the time scale increases. The variance of the differences between radar pixel rainfall and averaged point rainfall is close to zero, as the VRF for the 1-min scale is only 1.6%. It was found that four uniformly distributed rain stations can represent the radar pixel-scale rainfall with a VRF value of 5%, while eight rain stations are required to represent the radar rainfall with a VRF threshold of 2%.
- There is a difference in the spatial correlations of the convective and nonconvective rainfall, as the convective rainfall correlation decreases much faster than the nonconvective one. Further investigation is needed to understand the spatial and temporal differences between the different types of rainfall.

## Subpixel rainfall analysis from a dense gauge network

N. Peleg et al.

Title Page

Abstract

Introduction

Conclusions

References

Tables

Figures

◀

▶

◀

▶

Back

Close

Full Screen / Esc

Printer-friendly Version

Interactive Discussion



## Subpixel rainfall analysis from a dense gauge network

N. Peleg et al.

Title Page

Abstract

Introduction

Conclusions

References

Tables

Figures

◀

▶

◀

▶

Back

Close

Full Screen / Esc

Printer-friendly Version

Interactive Discussion



- The radar–rain gauge error is high for the 3-min time scale (about 700%) and decreases toward the daily time scale (65%). This error is mainly derived from radar estimation errors, as the gauge sampling error contributes only 12%–22% to the total error, depending on the time scale.
- The radar rainfall estimations improve with increasing time scale. This is reflected by the increasing CSI and POD parameters with time scale and the simultaneous decrease in the FAR parameter. In addition, the radar-to-true rainfall ratio, expressed by the scatter parameter, decreases with increasing time scale.

We intend to continue collecting rainfall measurements with this network of rain gauges in the years to come. In December 2012, a disdrometer was installed at this site to measure rain drop size distribution (following Jaffrain et al., 2011). We are looking for new and better ways to continue developing this network for future use with other weather radar or satellite observations.

*Acknowledgements.* The authors thank Kibbutz Galed for their valuable assistance and co-operation and also to Camille Vainstein for her editorial work. The research is supported by the Israeli Ministry of Environmental Protection and the Israel Science Foundation (grant no. 332/11).

## References

- Amitai, E., Unkrich, C. L., Goodrich, D. C., Habib, E., and Thill, B.: Assessing satellite-based rainfall estimates in semiarid watersheds using the USDA-ARS walnut gulch gauge network and TRMM PR, *J. Hydrometeorol.*, 13, 1579–1588, doi:10.1175/jhm-d-12-016.1, 2012. 5
- Arnaud, P., Lavabre, J., Fouchier, C., Diss, S., and Javelle, P.: Sensitivity of hydrological models to uncertainty in rainfall input, *Hydrol. Sci. J.-J. Sci. Hydrol.*, 56, 397–410, doi:10.1080/02626667.2011.563742, 2011. 3
- Berne, A. and Krajewski, W. F.: Radar for hydrology: Unfulfilled promise or unrecognized potential?, *Adv. Water Resour.*, doi:10.1016/j.advwatres.2012.05.005, in press, 2013. 3



- Karklinsky, M. and Morin, E.: Spatial characteristics of radar-derived convective rain cells over southern Israel, *Meteorol. Z.*, 15, 513–520, doi:10.1127/0941-2948/2006/0153, 2006. 8
- Krajewski, W. F., Kruger, A., and Nespor, V.: Experimental and numerical studies of small-scale rainfall measurements and variability, *Water Sci. Technol.*, 37, 131–138, doi:10.1016/s0273-1223(98)00325-4, 1998. 4
- Krajewski, W. F., Ciach, G. J., McCollum, J. R., and Bacotiu, C.: Initial validation of the global precipitation climatology project monthly rainfall over the United States, *J. Appl. Meteorol.*, 39, 1071–1086, doi:10.1175/1520-0450(2000)039<1071:ivotgp>2.0.co;2, 2000. 10, 13
- Krajewski, W. F. and Smith, J. A.: Radar hydrology: rainfall estimation, *Adv. Water Resour.*, 25, 1387–1394, doi:10.1016/s0309-1708(02)00062-3, 2002. 3
- Krajewski, W. F., Ciach, G. J., and Habib, E.: An analysis of small-scale rainfall variability in different climatic regimes, *Hydrol. Sci. J.*, 48, 151–162, doi:10.1623/hysj.48.2.151.44694, 2003. 3, 4, 6, 9
- Krajewski, W. F., Villarini, G., and Smith, J. A.: Radar-rainfall uncertainties – where are we after thirty years of effort?, *Bull. Amer. Meteorol. Soc.*, 91, 87–94, doi:10.1175/2009bams2747.1, 2010. 4
- Kyznarova, H. and Novak, P.: CELLTRACK – Convective cell tracking algorithm and its use for deriving life cycle characteristics, *Atmos. Res.*, 93, 317–327, doi:10.1016/j.atmosres.2008.09.019, 2009. 15
- Mandapaka, P. V., Villarini, G., Seo, B. C., and Krajewski, W. F.: Effect of radar-rainfall uncertainties on the spatial characterization of rainfall events, *J. Geophys. Res.-Atmos.*, 115, D17110, doi:10.1029/2009jd013366, 2010. 9
- Morin, E., Enzel, Y., Shamir, U., and Garti, R.: The characteristic time scale for basin hydrological response using radar data, *J. Hydrol.*, 252, 85–99, 2001. 8
- Morin, E., Goodrich, D. C., Maddox, R. A., Gao, X. G., Gupta, H. V., and Sorooshian, S.: Spatial patterns in thunderstorm rainfall events and their coupling with watershed hydrological response, *Adv. Water Resour.*, 29, 843–860, doi:10.1016/j.advwatres.2005.07.014, 2006. 2
- Morin, E. and Gabella, M.: Radar-based quantitative precipitation estimation over Mediterranean and dry climate regimes, *J. Geophys. Res.-Atmos.*, 112, D20108, doi:10.1029/2006jd008206, 2007. 8
- Morin, E., Jacoby, Y., Navon, S., and Bet-Halachmi, E.: Towards flash-flood prediction in the dry Dead Sea region utilizing radar rainfall information, *Adv. Water Resour.*, 32, 1066–1076, doi:10.1016/j.advwatres.2008.11.011, 2009. 8

---

## Subpixel rainfall analysis from a dense gauge network

N. Peleg et al.

---

[Title Page](#)[Abstract](#)[Introduction](#)[Conclusions](#)[References](#)[Tables](#)[Figures](#)[⏪](#)[⏩](#)[◀](#)[▶](#)[Back](#)[Close](#)[Full Screen / Esc](#)[Printer-friendly Version](#)[Interactive Discussion](#)



- Wang, J. X., Fisher, B. L., and Wolff, D. B.: Estimating rain rates from tipping-bucket rain gauge measurements, *J. Atmos. Ocean. Tech.*, 25, 43–56, doi:10.1175/2007jtecha895.1, 2008.6
- Wood, S. J., Jones, D. A., and Moore, R. J.: Accuracy of rainfall measurement for scales of hydrological interest, *Hydrol. Earth Syst. Sci.*, 4, 531–543, doi:10.5194/hess-4-531-2000, 2000.4
- 5 Yakir, H. and Morin, E.: Hydrologic response of a semi-arid watershed to spatial and temporal characteristics of convective rain cells, *Hydrol. Earth Syst. Sci.*, 15, 393–404, doi:10.5194/hess-15-393-2011, 2011.8
- 10 Zoccatelli, D., Borga, M., Viglione, A., Chirico, G. B., and Blöschl, G.: Spatial moments of catchment rainfall: rainfall spatial organisation, basin morphology, and flood response, *Hydrol. Earth Syst. Sci.*, 15, 3767–3783, doi:10.5194/hess-15-3767-2011, 2011.3

## Subpixel rainfall analysis from a dense gauge network

N. Peleg et al.

Title Page

Abstract

Introduction

Conclusions

References

Tables

Figures



Back

Close

Full Screen / Esc

Printer-friendly Version

Interactive Discussion





## Subpixel rainfall analysis from a dense gauge network

N. Peleg et al.

**Table 2.**  $Z$ – $R$  parameters ( $a$  and  $b$ ) for each radar pixel.  $\text{Sum}(R_r)$  represents the annual radar rainfall measurements after the adjustment and  $\text{Sum}(R_r R_t^{-1})$  is the ratio between annual radar rainfall and true rainfall derived from averaging the rain gauge measurements.

Radar ID	$a$	$b$	$\text{Sum}(R_r)$ (mm)	$\text{Sum}(R_r R_t^{-1})$
10 054	58	1.5	450.8	99.36 %
10 055	55	1.5	448.8	98.92 %
10 056	59	1.5	448.3	98.81 %
10 057	61	1.5	450.1	99.21 %
11 054	94	1.5	459.6	101.30 %
11 055	88	1.5	448.6	98.88 %
11 056	87	1.5	461.2	101.65 %
11 057	91	1.5	450.3	99.25 %
12 054	133	1.5	467.8	103.11 %
12 055	123	1.5	451.1	99.43 %
12 056	125	1.5	465.6	102.62 %
12 057	122	1.5	462.5	101.94 %

Title Page

Abstract

Introduction

Conclusions

References

Tables

Figures

◀

▶

◀

▶

Back

Close

Full Screen / Esc

Printer-friendly Version

Interactive Discussion



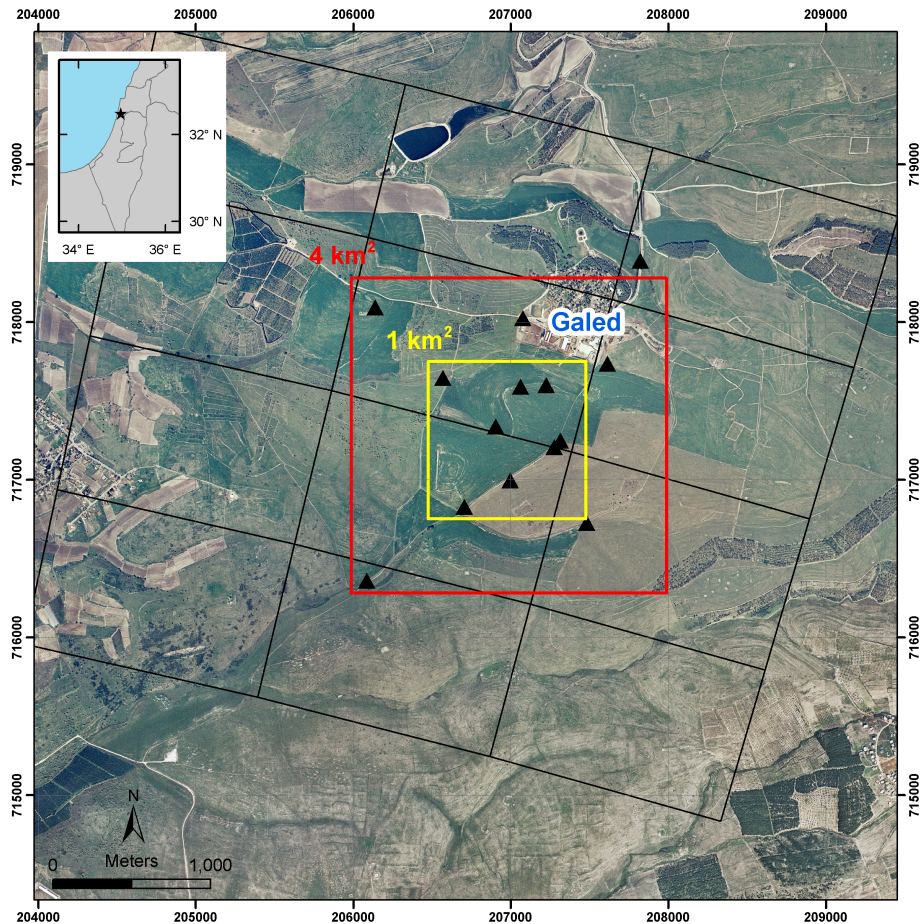


**Fig. 1.** Map of the study area including the 14 rain stations (triangles) around Kibbutz Galed. Each station is composed of two rain gauges. The black grid represents the radar mesh, with spatial polar resolution of  $1.4^\circ \times 1$  km. Inset shows the general location of the network in Israel.

## Subpixel rainfall analysis from a dense gauge network

N. Peleg et al.

Title Page

Abstract

Introduction

Conclusions

References

Tables

Figures

◀

▶

◀

▶

Back

Close

Full Screen / Esc

Printer-friendly Version

Interactive Discussion



---

**Subpixel rainfall analysis from a dense gauge network**

N. Peleg et al.

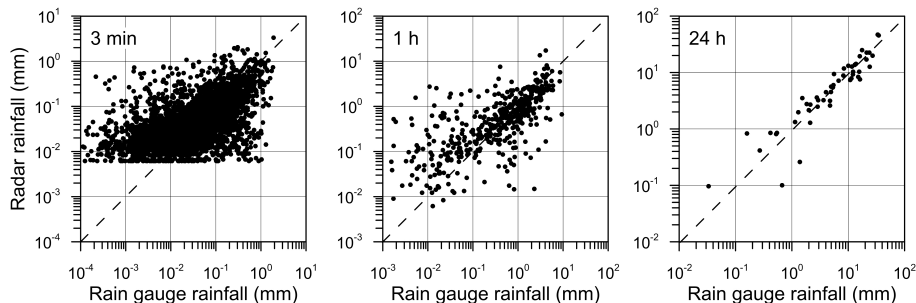


**Fig. 2.** Scatter plots of synchronous radar and rain gauge observations for 3-min (radar data are transected along the lower  $0.1 \text{ mm h}^{-1}$  rainfall intensity threshold), hourly and daily intervals. The radar rainfall data represent the averaged rainfall derived from the 12 radar pixels. Dashed line represents a perfect fit between gauge and radar rainfall.

[Title Page](#)[Abstract](#)[Introduction](#)[Conclusions](#)[References](#)[Tables](#)[Figures](#)[◀](#)[▶](#)[◀](#)[▶](#)[Back](#)[Close](#)[Full Screen / Esc](#)[Printer-friendly Version](#)[Interactive Discussion](#)

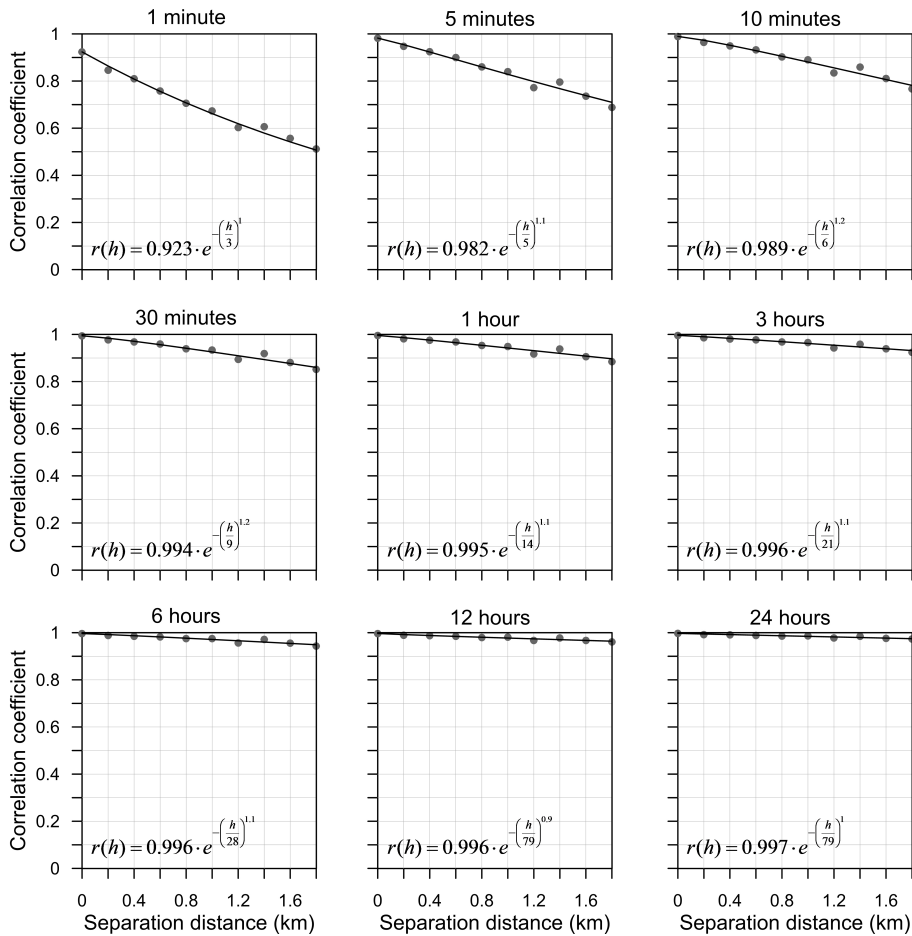


**Fig. 3.** Correlograms of the rainfall derived from the rain gauges for several time scales (dots) and the fitted three-parameter exponential functions (lines).

## Subpixel rainfall analysis from a dense gauge network

N. Peleg et al.

Title Page

Abstract

Introduction

Conclusions

References

Tables

Figures

◀

▶

◀

▶

Back

Close

Full Screen / Esc

Printer-friendly Version

Interactive Discussion



---

**Subpixel rainfall analysis from a dense gauge network**

N. Peleg et al.

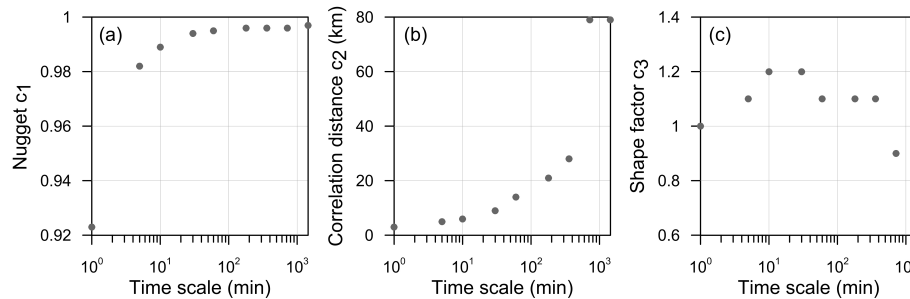


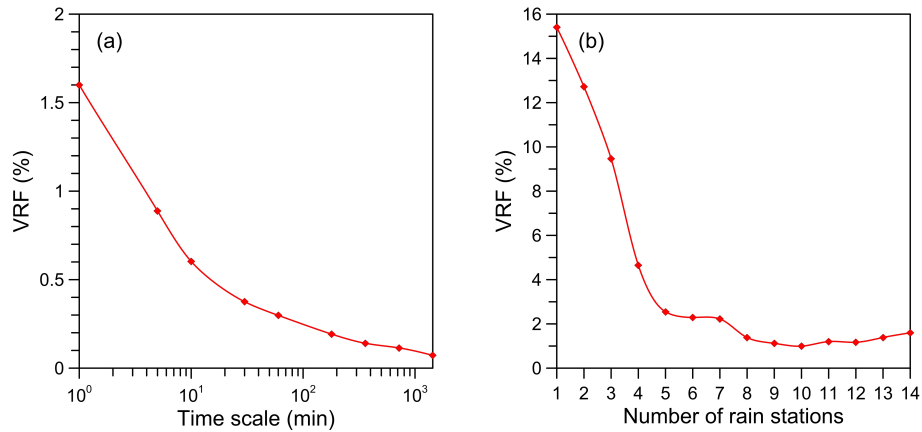
**Fig. 4.** Time-scale dependence of the nugget (a), correlation distance (b) and shape factor (c) used in the three-parameter exponential function.

[Title Page](#)[Abstract](#)[Introduction](#)[Conclusions](#)[References](#)[Tables](#)[Figures](#)[◀](#)[▶](#)[◀](#)[▶](#)[Back](#)[Close](#)[Full Screen / Esc](#)[Printer-friendly Version](#)[Interactive Discussion](#)

---

**Subpixel rainfall analysis from a dense gauge network**

N. Peleg et al.

[Title Page](#)[Abstract](#)[Introduction](#)[Conclusions](#)[References](#)[Tables](#)[Figures](#)[◀](#)[▶](#)[◀](#)[▶](#)[Back](#)[Close](#)[Full Screen / Esc](#)[Printer-friendly Version](#)[Interactive Discussion](#)

**Fig. 5.** Variance reduction factor (VRF) as a function of **(a)** time scale and **(b)** number of rain stations in the study area for the 1-min time scale.

**Subpixel rainfall analysis from a dense gauge network**

N. Peleg et al.

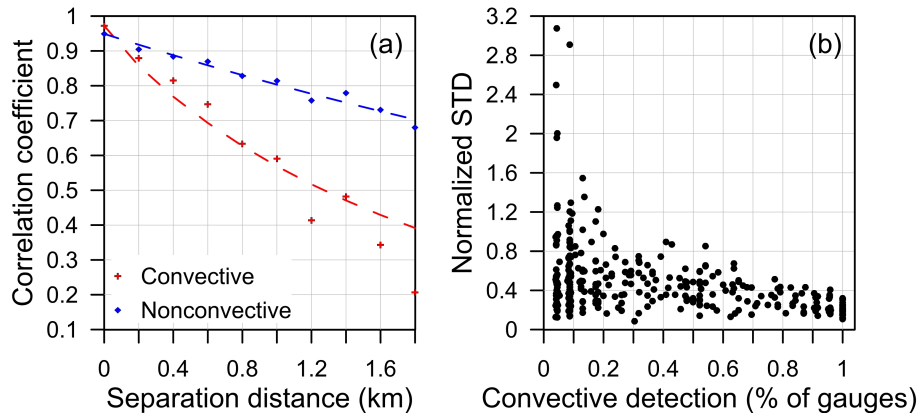


**Fig. 6.** (a) Correlogram presenting the convective (red plus symbol) and nonconvective (blue dots) spatial rainfall coefficient and its fit (dashed lines) using the three-parameter exponential functions. (b) Convective rain intensity normalized standard deviation. The analysis was performed for the 5-min rain intensity data.

[Title Page](#)[Abstract](#)[Introduction](#)[Conclusions](#)[References](#)[Tables](#)[Figures](#)[◀](#)[▶](#)[◀](#)[▶](#)[Back](#)[Close](#)[Full Screen / Esc](#)[Printer-friendly Version](#)[Interactive Discussion](#)

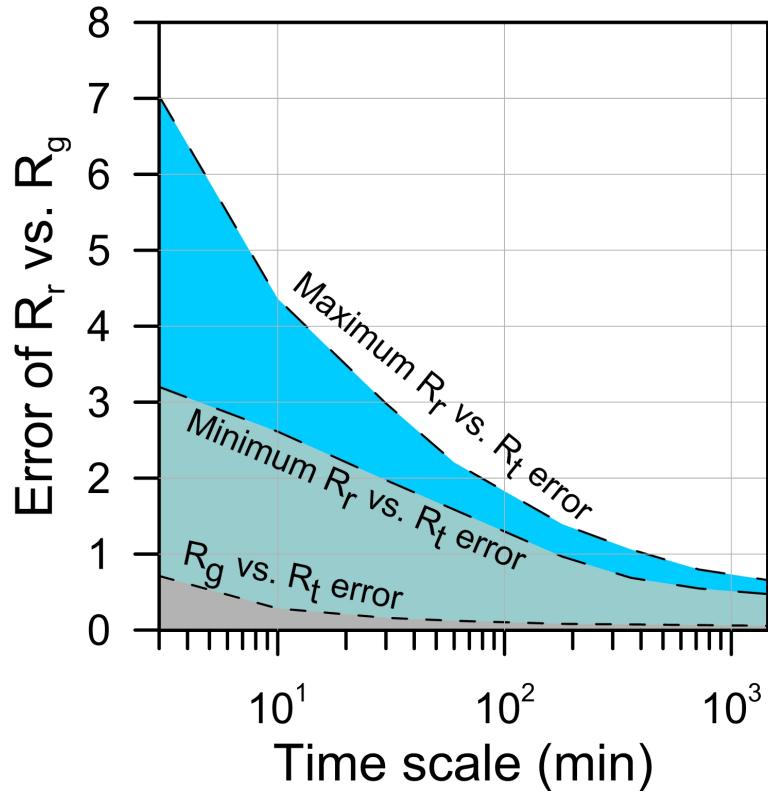


**Fig. 7.** Errors of radar ( $R_r$ ) vs. gauge ( $R_g$ ) rainfall for different time scales. Gray section represents the spatial sampling error derived from the rain gauge ( $R_g$ ) vs. true areal rainfall ( $R_t$ ). Blue sections represent the maximum and minimum normalized root mean square error of radar ( $R_r$ ) vs. true rainfall ( $R_t$ ) derived from the 12 radar pixels.

**Subpixel rainfall analysis from a dense gauge network**

N. Peleg et al.

Title Page

Abstract Introduction

Conclusions References

Tables Figures

◀ ▶

◀ ▶

Back Close

Full Screen / Esc

Printer-friendly Version

Interactive Discussion



**Subpixel rainfall analysis from a dense gauge network**

N. Peleg et al.

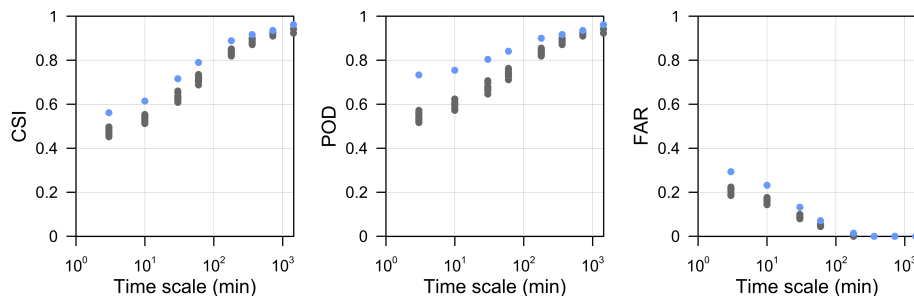


**Fig. 8.** Critical success index (CSI), probability of detection (POD) and false alarm ratio (FAR) for the different time scales. Gray dots represent the radar pixels and blue dots represent the averaged radar pixels.

[Title Page](#)[Abstract](#)[Introduction](#)[Conclusions](#)[References](#)[Tables](#)[Figures](#)[◀](#)[▶](#)[◀](#)[▶](#)[Back](#)[Close](#)[Full Screen / Esc](#)[Printer-friendly Version](#)[Interactive Discussion](#)

## Subpixel rainfall analysis from a dense gauge network

N. Peleg et al.

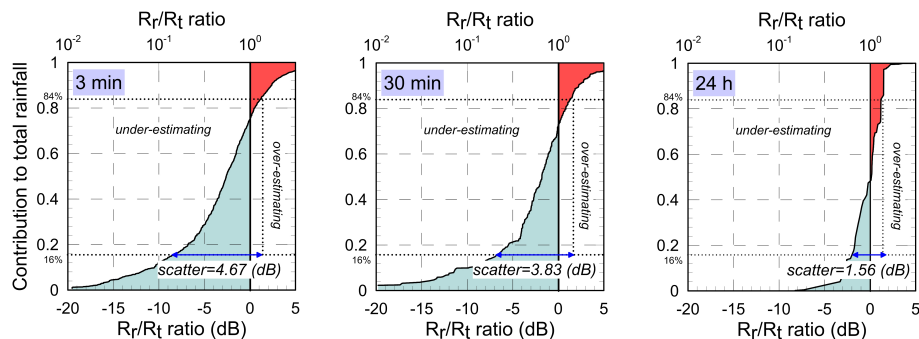


**Fig. 9.** Cumulative distribution (weighted by contribution to total rain amount) of the radar-to-true rainfall ratio ( $R_r/R_t$ , in dB) (see Germann et al., 2006) for different time scales.

Title Page

Abstract

Introduction

Conclusions

References

Tables

Figures

◀

▶

◀

▶

Back

Close

Full Screen / Esc

Printer-friendly Version

Interactive Discussion

